


Nonlinear harmonic generation in two-dimensional lattices of repulsive magnetsWeijian Jiao^{✉*} and Stefano Gonella[†]*Department of Civil, Environmental, and Geo-Engineering, University of Minnesota, Minneapolis, Minnesota 55455, USA* (Received 19 August 2020; accepted 6 December 2020; published 20 January 2021)

In this work, we provide experimental evidence of nonlinear wave propagation in a triangular lattice of repulsive magnets supported by an elastic foundation of thin pillars, and we interpret all the individual features of the nonlinear wave field through the lens of a phonon band calculation that precisely accounts for the interparticle repulsive forces. We confirm the coexistence of two spectrally distinct components (homogeneous and forced) in the wave response that is induced via second harmonic generation (SHG) as a result of the quadratic nonlinearity embedded in the magnetic interaction. The detection of the forced component, specifically, allows us to attribute unequivocally the generation of harmonics to the nonlinear mechanisms germane to the lattice. We show that the spatial characteristics of the second harmonic components are markedly different from those exhibited by the fundamental harmonic. This endows the lattice with a functionality enrichment capability, whereby additional modal characteristics and directivity patterns can be triggered and tuned by merely increasing the amplitude of excitation.

DOI: [10.1103/PhysRevE.103.012213](https://doi.org/10.1103/PhysRevE.103.012213)

In recent years, nonlinear periodic structures and acoustic metamaterials have been extensively studied because of their rich dynamical behavior and for their tunability and adaptivity capabilities. A number of studies have focused on the propagation of solitary waves and discrete breathers in a variety of material systems, such as granular crystals [1–4], in which different regimes of weak and strong nonlinearities can be selected by controlling the magnitude of precompression, magnetic systems [5–7], and mechanical metamaterials [8–10]. Other notable works have explored metastructures equipped with bistable or bucklable elements and exhibiting tuning and energy harvesting functionalities [11–14].

Our attention here is on the opportunities for tunability and functionality enrichment available in weakly nonlinear systems, in which the nonlinear effects can be seen as a perturbation of a baseline linear behavior. In systems with cubic nonlinearity, the main manifestation of nonlinearity is an amplitude-dependent correction of the dispersion relation, which, in principle, enables shifting the branches frequency cutoffs and the onset and width of band gaps via a simple control of the excitation amplitude [15–18]. Recently, this tuning effect has been employed to control edge states in topological phononic lattices [19]. Another nonlinear effect of great relevance is second harmonic generation (SHG); this is the main signature of quadratic nonlinearity, which often represents the dominant nonlinear contribution in many physical systems [17,20–28]. Harnessing harmonic generation in nonlinear acoustic metamaterials has opened new doors for a broad range of applications, including acoustic diodes and switches [29,30], subwavelength energy trapping [25], and adaptive spatial directivity [31]. The opportunity spectrum

becomes even wider if we consider systems that feature simultaneously cubic and quadratic nonlinearities, where the correction of the band diagram induced by the cubic nonlinearity affects indirectly the manifestation of SHG, providing a secondary tuning capability, as recently shown in [32].

While SHG has been widely studied in weakly one-dimensional nonlinear metamaterials and waveguides, the investigation of its effects on the spatial characteristics of nonlinear wave fields in two-dimensional (2D) metamaterials has been more sporadic [26,31]. The phenomenon still lacks a definitive experimental observation at amplitude levels that are suitable for practical applications often involving point-source excitations. A major challenge is that phase matching conditions, which have been shown to be essential to harness strong SHG signatures in mechanical structures [21,25], cannot be effectively established in 2D structures subjected to point excitations. In this work, we attempt to provide unequivocal experimental evidence of SHG triggered by point excitations in a discrete system consisting of a 2D periodic network of magnets supported by an elastic foundation of thin pillars. The system can be interpreted as a practical realization of a triangular lattice of particles with on-site potentials. We first verify the existence of SHG in the spectrum of the response. Here, the extraction and interpretation of a clear signature of SHG is favored by the discrete nature of the magnetic system, which features higher compliance and lower modal complexity compared to structural lattices made of hard solids, such as those used in past experimental efforts with similar objectives [31]. The compliance leads to the observation of appreciable nonlinear signatures, within the bounds of weak nonlinearity, even without the establishment of phase matching conditions. Moreover, we experimentally confirm that the second harmonic encompasses two contributions, customarily referred to as the forced and homogeneous components [24,26]. Finally, we show that the second harmonic

*jiaox085@umn.edu

†sgonella@umn.edu

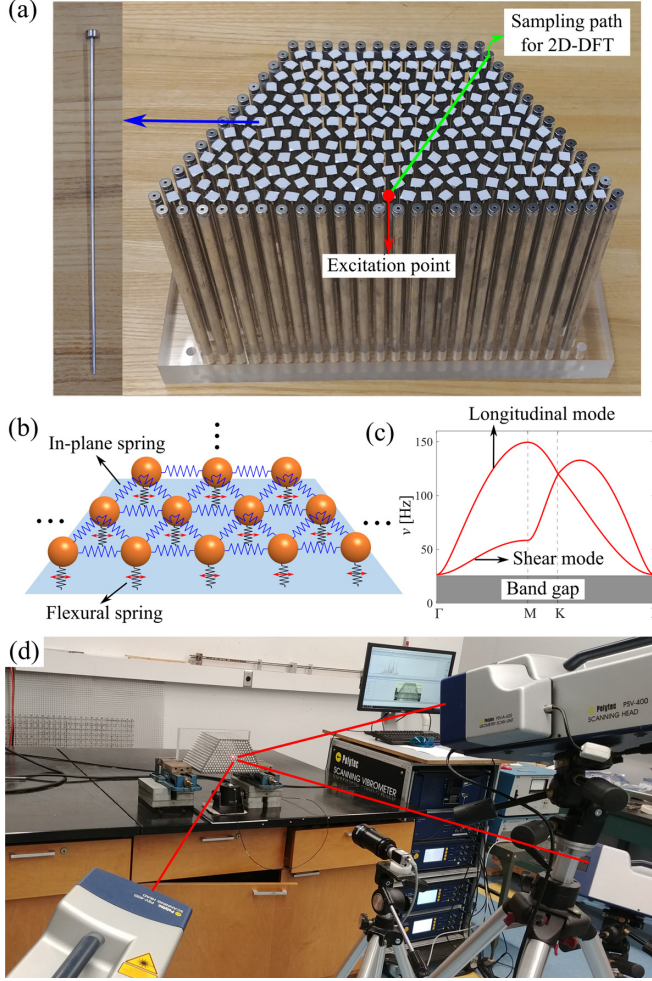


FIG. 1. (a) Lattice specimen consisting of magnets supported by thin beams in the interior (shown in the inset) and thick beams along the boundary. The interior magnets are covered by reflective patches of tapes to enhance the laser measurements. (b) Equivalent spring-mass model of the lattice, showing the function of the pillars acting as an elastic foundation. (c) Linear dispersion relation obtained from the analytical model in [33], accounting for the effect of the static interparticle repulsive forces. (d) Experimental setup.

features distinctive modal and spatial characteristics that are markedly different from those of the fundamental harmonic.

The specimen used for our tests, shown in Fig. 1(a), consists of an array of pillars arranged to form a triangular lattice occupying a half-hexagonal domain. Each pillar in the interior lattice consists of a magnetic ring (Grade N42, with 1/4 inch outer diameter, 1/16 inch inter diameter and 1/8 inch thickness) inserted at the tip of a slender aluminum beam (1/16 inch in diameter) whose other end is plugged into an acrylic base through a drilled hole. For the exterior pillars, the magnets are simply glued to the tips of thick beams (1/4 inch in diameter) also plugged into the base and featuring large bending stiffness to effectively establish fixed boundary conditions along the contour of the hexagonal domain. The magnets are arranged to experience side-by-side repulsive interactions in their own plane, and each magnet is initially in equilibrium under the action of the self-balancing static forces

exerted by its neighbors. The configuration guarantees that, for the amplitudes of interest for this study, the motion of the magnets remains confined within the plane of the lattice. This setup is imported and adapted from a previous experimental effort, in which we used this platform to characterize the linear response of lattices of magnetically interacting particle systems [33]. By means of those experiments, we were able to demonstrate a series of nonintuitive effects induced on the lattice dispersive properties by the static interparticle repulsive forces. In this work, we leverage these key results as a precious guideline for the nonlinear investigation.

As shown in Fig. 1(b), the system is modeled as a triangular spring-mass lattice in which each node is connected to ground through a flexural spring that captures the elastic foundation effect of the supporting beam. The in-plane repulsive interaction between neighboring magnets is modeled as a nonlinear spring featuring an inverse power law $f(r) = \beta r^{-\alpha}$, with $\alpha = 4.5824$ and $\beta = 1.6209 \times 10^{-10}$. Here, the parameters have been obtained by fitting the force-displacement relation between two magnets acquired experimentally through a micrometer equipped with a highly sensitive load cell (details available in the Supplemental Material of [33]). The spring constant of the flexural springs in the foundation is taken as the equivalent flexural stiffness of a cantilever beam with the cross sectional and material properties of the pillar, and found to be $k_f = 19.6757$ N/m. As for the other parameters, $m = 7.07 \times 10^{-4}$ kg is the mass of each magnet and $L_0 = 0.01$ m is the initial spacing between two nodes in the lattice. In [33], we have shown that the repulsive forces between pairs of magnets provide a twofold contribution to the linear stiffness of the lattice. Specifically, the band diagram can be obtained by solving the following eigenvalue problem:

$$[-\omega^2 \mathbf{M} + \mathbf{D}(\mathbf{k})] \boldsymbol{\phi} = \mathbf{0} \quad (1)$$

where $\omega = 2\pi\nu$ is the angular frequency, \mathbf{k} is the wave vector, $\mathbf{M} = \begin{bmatrix} m & 0 \\ 0 & m \end{bmatrix}$ is the mass matrix, and

$$\begin{aligned} \mathbf{D}(\mathbf{k}) = & 2 \sum_{l=1}^3 \{ f_r(L_0) \mathbf{e}_l \otimes \mathbf{e}_l [\cos(\mathbf{k} \cdot \mathbf{R}_l) - 1] \} \\ & + 2 \sum_{l=1}^3 \left\{ \frac{f(L_0)}{L_0} (\mathbf{I} - \mathbf{e}_l \otimes \mathbf{e}_l) [\cos(\mathbf{k} \cdot \mathbf{R}_l) - 1] \right\} + \mathbf{K}_f \end{aligned} \quad (2)$$

is a wave-vector-dependent stiffness matrix that already incorporates Bloch conditions, where $\mathbf{R}_1 = L_0 \mathbf{e}_1 = L_0 [1 \ 0]^T$, $\mathbf{R}_2 = L_0 \mathbf{e}_2 = L_0 [1/2 \ \sqrt{3}/2]^T$, and $\mathbf{R}_3 = L_0 \mathbf{e}_3 = L_0 [-1/2 \ \sqrt{3}/2]^T$ are the lattice vectors. In Eq. (2), the first term is the conventional stiffness matrix for a generic 2D spring-mass system, where $f_r(L_0)$ is the first derivative of the repulsive force $f(r)$ evaluated at the initial internodal spacing L_0 . The second term is an additional stiffness contribution stemming from the static repulsive forces that is uniquely germane to two-dimensional configurations.

Finally, $\mathbf{K}_f = \begin{bmatrix} k_f & 0 \\ 0 & k_f \end{bmatrix}$ captures the stiffness of the elastic foundation. The solution of Eq. (1) yields the band diagram plotted in Fig. 1(c). As expected, the band diagram is fully gapped at low frequencies as a result of the elastic foundation,

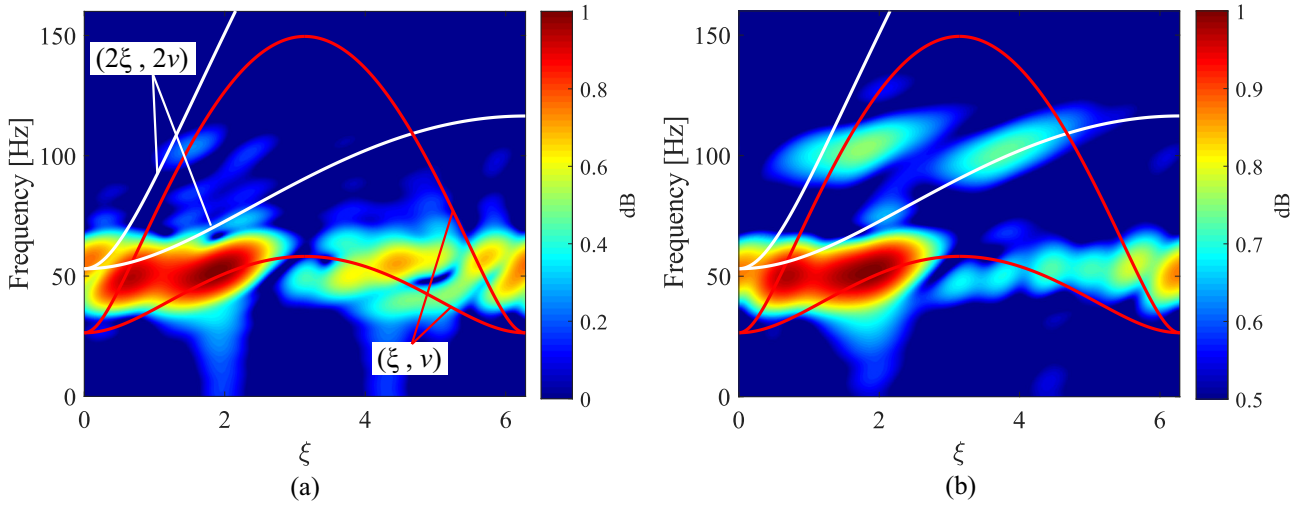


FIG. 2. Normalized amplitude spectra of the experimental responses for tone-burst excitations at 50 Hz. (a) Response to low-amplitude excitation, showing the fundamental harmonic activating both shear and longitudinal modes (red solid curves). (b) Response to high-amplitude excitation, showing two distinct signatures at the second harmonic (i.e., 100 Hz), confirming the existence of both homogeneous and forced components of the nonlinearly generated harmonic. The white curves represent all the possible spectral points that can be activated by the forced component.

and we observe the two canonical acoustic branches, the first dominated by shear mechanisms and the second by longitudinal mechanisms.

We now proceed to investigate the nonlinear response. The experimental setup, shown in Fig. 1(d), involves around a 3D scanning laser Doppler vibrometer (SLDV, Polytec PSV-400-3D) used to experimentally capture the in-plane response of the lattice. Specifically, we measure the in-plane components of the velocity vector of each magnet in the interior of the lattice. The specimen is excited in the vertical direction by a force applied to the center magnet of the bottom layer [as indicated by the red dot in Fig. 2(a)] through a Bruel & Kjaer Type 4809 shaker, powered by a Bruel & Kjaer Type 2718 amplifier. The excitation is prescribed as a five-cycle tone burst with carrier frequency $\nu_0 = 50$ Hz. First, we prescribe a low-amplitude excitation to elicit a linear response of the specimen. With this reference excitation, we measure the amplitude of the vertical velocity at the excitation point to be equal to 0.03524 mm/s. In Fig. 2(a), we plot the color map of the normalized spectral amplitude obtained via 2D discrete Fourier transform (2D-DFT) in space and time of the horizontal components of the spatio-temporal response, sampled along one lattice vector [i.e., along the green line shown in Fig. 1(a)]. Here, and in all the subsequent spectral amplitude plots, we normalize the spectral amplitude by its maximum value in dB.

At this point, we progressively raise the amplitude of excitation, up to a level where the measured amplitude of the vertical velocity at the excitation point reaches 0.4004 mm/s, which is one order of magnitude larger than the reference case (see Movie S1 in the Supplemental Material [34] for the actual displacement field, which can be appreciated even by naked-eye inspection). We plot the corresponding normalized spectral amplitude map in Fig. 2(b), in which we increase the lower bound of the color bar to filter out some spurious features and improve visualization. In both figures, we su-

perimpose the Γ -M portion of the linear dispersion branches (red curves) obtained via Bloch analysis of the equivalent lattice model and periodically extended to the second Brillouin zone. The white curves denote the parametric locus of the $2\xi-2\nu(\xi)$ pairs, i.e., the spectral points that feature simultaneously twice the frequency and twice the wave number of the acoustic phonons at the fundamental harmonic $(\xi, \nu(\xi))$. Here ξ is the nondimensional wave number defined as $\xi = kL_0$, where k is the wave number along the Γ -M direction. The $2\xi-2\nu(\xi)$ points represent the frequency-wave-number pairs that can be displayed by the forced component of a nonlinearly generated second harmonic. Since these pairs do not live on any dispersion branch (and therefore do not conform to any mode of the linear system), their activation is conditional upon the nonlinear generation of harmonics. In other words, the phonons that live on these curves must be generated through nonlinear mechanisms that are intrinsic to the lattice and cannot be merely induced by a component of the excitation with a 2ν frequency content, as such a component would also necessarily result in the activation of the linear dispersion branch(es) available at that frequency. This consideration provides a powerful tool to distinguish with absolute certainty the manifestation of nonlinearly generated harmonics from the signatures of high-frequency components that may be embedded by default in the excitation signal (for example due to nonlinearities in the signal generation and amplification). In essence, the ability to capture the forced response is the most robust detector of nonlinearity in the lattice. As expected, in Fig. 2(a) we observe that the main spectral contribution is located at the prescribed frequency ($\nu_0 = 50$ Hz), where both the shear and longitudinal modes are activated, with no appreciable signature at the second harmonic ($2\nu_0 = 100$ Hz). In contrast, in the spectrum of the nonlinear response [i.e., Fig. 2(b)] we recognize two additional spectral signatures at the second harmonic. The one overlapping the longitudinal branch corresponds to the

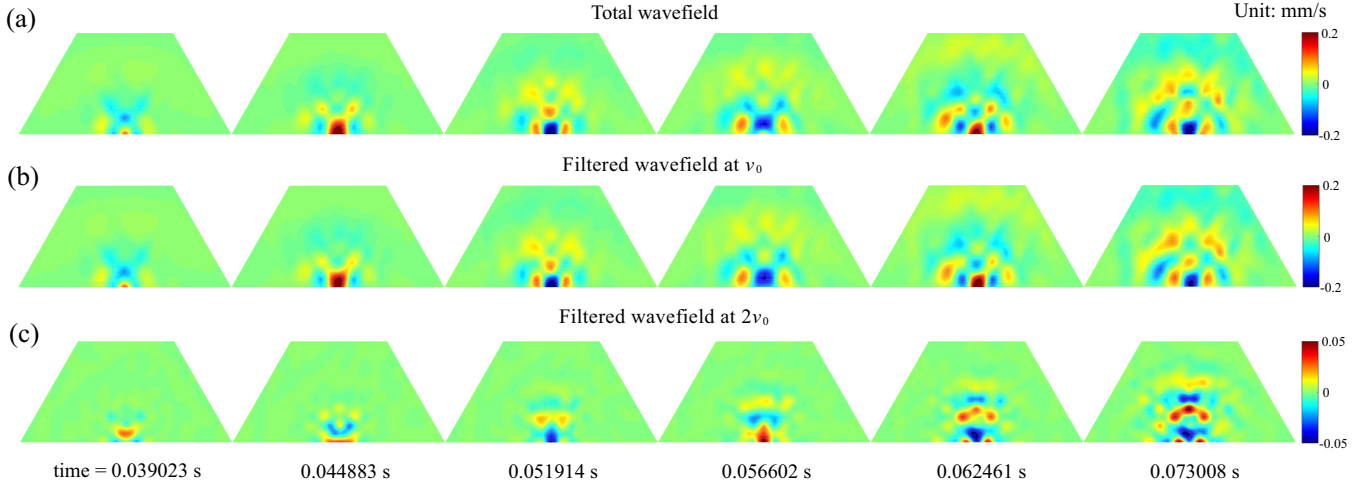


FIG. 3. Snapshots of the wave fields experimentally acquired by laser scans at six successive time instants, showing distinct spatial patterns at the different harmonics. (a) Total wave field. (b) Wave field filtered at ν_0 , highlighting the fundamental harmonic. (c) Wave field filtered at $2\nu_0$, highlighting the second harmonic. The two harmonics feature complementary directional characteristics, thus exposing the functionality enrichment that is achieved by triggering a nonlinear response.

homogeneous component, while the one that lies precisely on the white curve is unequivocally identified as the forced component.

The spectral maps presented in Fig. 2 also provide insight in the different modal makeups of the fundamental and second harmonics. The fundamental harmonic blends both shear and longitudinal (S and P) modes, activated at comparable amplitude level (with an expected preference for the S mode due to the higher compliance of the shear mechanisms), resulting in a hybrid polarization. At the second harmonic, the response also comprises two distinct contributions. The first, activated by the homogeneous component, involves the excitation of the P mode in a higher-frequency and shorter-wavelength regime, and is therefore dominated by longitudinal characteristics. The second is the forced component, whose polarization is predominantly dictated by the shear characteristics of the fundamental harmonic that drives it, but does not conform to any linear modes *per se*. In essence, the response at the second harmonic also features a blend of distinct modal characteristics. The relative participation of these components in the response is, however, different and not exclusively controlled by the modal landscape at 2ν . We can characterize this result as an instance of modal enhancement, whereby the nonlinear activation of the second harmonic induces additional modal attributes to the response, perturbing the original modal makeup of the linear response.

The vibrometer scan also allows exploring the manifestation of SHG on the spatial pattern of the wave response. In Fig. 3, we plot six snapshots of the propagating wave field using the vertical components of the measured velocities. In Fig. 3(a), we show the total wave field, encompassing fundamental and second harmonics, while in Figs. 3(b) and 3(c) we isolate the filtered components at ν_0 and $2\nu_0$, respectively. The wave fields reveal spatial complementarity between the predominantly vertical directivity of the second harmonic and the quasiisotropic pattern of the fundamental harmonic. This result indicates that nonlinearity is responsible for a directivity enrichment.

To highlight separately the spatial contributions of the homogeneous and forced components, we subject the last snapshot of the wave field filtered at $2\nu_0$ [last frame in Fig. 3(c)] to 2D-DFT in space. The resulting \mathbf{k} -space normalized spectrum is plotted in Fig. 4(a). For comparison, we repeat the exercise for a linear wave field obtained with a low-amplitude excitation prescribed directly at $2\nu_0$ [Fig. 4(e)], whose normalized spectrum is shown in Fig. 4(b). In Fig. 4(a), we identify two distinct spectral signatures at the second harmonic (appearing with their mirror counterparts due to the symmetry of the wave field and the folding operations involved in the 2D-DFT). The dominant component, inscribed by magenta boxes, is consistent with the spectrum of the linear wave field excited directly at $2\nu_0$ [i.e., Fig. 4(b)], and is therefore interpreted as the homogeneous component. On the other hand, the secondary contribution, inscribed by amber boxes, which is unique to the nonlinear response, must be interpreted

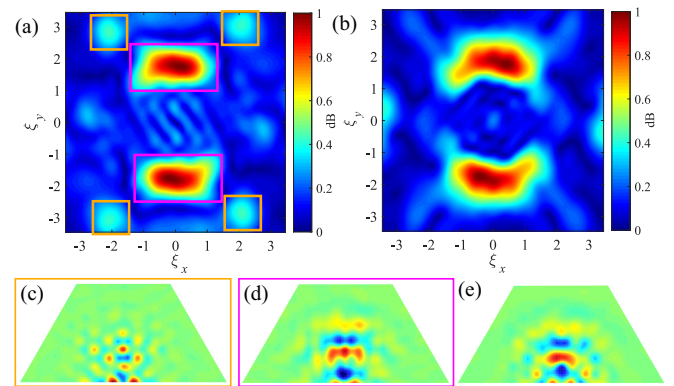


FIG. 4. \mathbf{k} -plane normalized amplitude spectra of (a) the filtered second harmonic of a nonlinear response and (b) a linear wave field excited directly at $2\nu_0$. (c) and (d) Filtered wave fields of the forced and homogeneous components inscribed in amber and magenta boxes, respectively. (e) Linear wave field used to obtain the spectrum shown in (b).

as the forced response. By zeroing out the two signatures, one at a time, and carrying out an inverse 2D-DFT of the remainder, we can filter out the separate wave fields of the two components, as shown in Figs. 4(c) and 4(d), respectively. Clearly, the pattern in the magenta box of Fig. 4(d), which exhibits longitudinal behavior, is reminiscent of the wave field in Fig. 4(e), further supporting, from a spatial perspective, the notion that the homogeneous component conforms to the linear response that would be observed in the lattice if the excitation were prescribed directly at $2\nu_0$. The other, shown in Fig. 4(c) and corresponding to the forced component, displays a more dispersive spatial pattern. It is worth emphasizing again that, while it is possible that the homogeneous component may be in part triggered by nonlinearities extrinsic to the mechanical system and due, for instance, to harmonics buried in the excitation signal, the forced component is uniquely germane to the SHG established within the structure.

In summary, we have experimentally characterized the nonlinear wave response of a two-dimensional lattice of repulsive magnets on an elastic foundation. First, we have documented the onset of SHG, separately pinpointing the two components of the second harmonic. Then, we have

shown the functionality of modal enhancement achieved in the nonlinear response through SHG. Moreover, we have documented the directivity differences between the complementary spatial characteristics of the homogeneous and forced nonlinear components. Magnetic lattice prototypes emerge from this study as ideal platforms for the experimental observation of nonlinear wave phenomena. On one hand, their compliance is conducive to response amplitudes that are at least one order of magnitude larger than what is achievable in hard solid specimens, thus approaching the advantages of soft material specimens without their pitfalls in terms of damping. On the other hand, their discrete nature results in low modal complexity, compared to a structural lattice, thus facilitating a clear identification of all the relevant spectral components.

This work is supported by the National Science Foundation (CAREER Award No. CMMI-1452488). The authors are indebted to Lijuan Yu for her precious help with the specimen assembly and to Joseph Labuz, Xiaoran Wang and Chen Hu for sharing their invaluable expertise with the force-displacement testing apparatus.

-
- [1] C. Daraio, V. F. Nesterenko, E. B. Herbold, and S. Jin, *Phys. Rev. E* **72**, 016603 (2005).
 - [2] C. Daraio, V. F. Nesterenko, E. B. Herbold, and S. Jin, *Phys. Rev. E* **73**, 026610 (2006).
 - [3] A. Leonard, F. Fraternali, and C. Daraio, *Exp. Mech.* **53**, 327 (2013).
 - [4] N. Boechler, G. Theocharis, S. Job, P. G. Kevrekidis, M. A. Porter, and C. Daraio, *Phys. Rev. Lett.* **104**, 244302 (2010).
 - [5] F. M. Russell, Y. Zolotaryuk, J. C. Eilbeck, and T. Dauxois, *Phys. Rev. B* **55**, 6304 (1997).
 - [6] M. Molerón, A. Leonard, and C. Daraio, *J. Appl. Phys.* **115**, 184901 (2014).
 - [7] M. Molerón, C. Chong, A. J. Martínez, M. A. Porter, P. G. Kevrekidis, and C. Daraio, *New J. Phys.* **21**, 063032 (2019).
 - [8] B. G. Chen, N. Upadhyaya, and V. Vitelli, *Proc. Natl. Acad. Sci. USA* **111**, 13004 (2014).
 - [9] B. Deng, J. R. Raney, V. Tournat, and K. Bertoldi, *Phys. Rev. Lett.* **118**, 204102 (2017).
 - [10] B. Deng, P. Wang, Q. He, V. Tournat, and K. Bertoldi, *Nat. Commun.* **9**, 3410 (2018).
 - [11] T. Mullin, S. Deschanel, K. Bertoldi, and M. C. Boyce, *Phys. Rev. Lett.* **99**, 084301 (2007).
 - [12] P. Wang, F. Casadei, S. Shan, J. C. Weaver, and K. Bertoldi, *Phys. Rev. Lett.* **113**, 014301 (2014).
 - [13] N. Nadkarni, A. F. Arrieta, C. Chong, D. M. Kochmann, and C. Daraio, *Phys. Rev. Lett.* **116**, 244501 (2016).
 - [14] S. Shan, S. H. Kang, J. R. Raney, P. Wang, L. Fang, F. Candido, J. A. Lewis, and K. Bertoldi, *Adv. Mater.* **27**, 4296 (2015).
 - [15] R. Narisetti, M. Leamy, and M. Ruzzene, *ASME J. Vib. Acoust.* **132**, 031001 (2010).
 - [16] R. Narisetti, M. Ruzzene, and M. Leamy, *ASME J. Vib. Acoust.* **133**, 061020 (2011).
 - [17] J. Cabaret, V. Tournat, and P. Béquin, *Phys. Rev. E* **86**, 041305 (2012).
 - [18] L. Bonanomi, G. Theocharis, and C. Daraio, *Phys. Rev. E* **91**, 033208 (2015).
 - [19] R. K. Pal, J. Vila, M. Leamy, and M. Ruzzene, *Phys. Rev. E* **97**, 032209 (2018).
 - [20] V. Tournat, V. E. Gusev, V. Y. Zaitsev, and B. Castagnede, *Europhys. Lett.* **66**, 798 (2004).
 - [21] K. H. Matlack, J. Y. Kim, L. J. Jacobs, and J. Qu, *J. Appl. Phys.* **109**, 014905 (2011).
 - [22] V. J. Sánchez-Morcillo, I. Pérez-Arjona, V. Romero-García, V. Tournat, and V. E. Gusev, *Phys. Rev. E* **88**, 043203 (2013).
 - [23] A. Mehrem, N. Jiménez, L. J. Salmerón-Contreras, X. García-Andrés, L. M. García-Raffi, R. Picó, and V. J. Sánchez-Morcillo, *Phys. Rev. E* **96**, 012208 (2017).
 - [24] W. Jiao and S. Gonella, *J. Mech. Phys. Solids* **111**, 1 (2018).
 - [25] W. Jiao and S. Gonella, *Phys. Rev. Appl.* **10**, 024006 (2018).
 - [26] R. Ganesh and S. Gonella, *J. Mech. Phys. Solids* **99**, 272 (2017).
 - [27] S. Wallen and N. Boechler, *Wave Motion* **68**, 22 (2017).
 - [28] I. Grinberg and K. Matlack, *Wave Motion* **93**, 102466 (2020).
 - [29] B. Liang, X. Guo, J. Tu, D. Zhang, and J. C. Cheng, *Nat. Mater.* **9**, 989 (2010).
 - [30] N. Boechler, G. Theocharis, and C. Daraio, *Nat. Mater.* **10**, 665 (2011).
 - [31] R. Ganesh and S. Gonella, *Appl. Phys. Lett.* **110**, 084101 (2017).
 - [32] W. Jiao and S. Gonella, *Phys. Rev. E* **99**, 042206 (2019).
 - [33] W. Jiao and S. Gonella, *Phys. Rev. B* **102**, 054304 (2020).
 - [34] See Supplemental Material at <http://link.aps.org/supplemental/10.1103/PhysRevE.103.012213> for the actual displacement field of the specimen under a high-amplitude excitation.